MNRAS **476,** 1654–1662 (2018)
Advance Access publication 2018 February 5
doi:10.1093/mnras/sty289

The population of single and binary white dwarfs of the Galactic bulge

S. Torres,[1,2]★ E. García–Berro,[1,2]† R. Cojocaru[1,2] and A. Calamida[3]★

[1]*Departament de Física, Universitat Politècnica de Catalunya, c/Esteve Terrades 5, E-08860 Castelldefels, Spain*
[2]*Institute for Space Studies of Catalonia, c/Gran Capità 2–4, Edif. Nexus 201, E-08034 Barcelona, Spain*
[3]*Space Telescope Science Institute, 3700 San Martin Drive, Baltimore, MD 21218, USA*

Accepted 2018 January 31. Received 2018 January 31; in original form 2017 June 27

ABSTRACT

Recent *Hubble Space Telescope* observations have unveiled the white dwarf cooling sequence of the Galactic bulge. Although the degenerate sequence can be well fitted employing the most up-to-date theoretical cooling sequences, observations show a systematic excess of red objects that cannot be explained by the theoretical models of single carbon–oxygen white dwarfs of the appropriate masses. Here, we present a population synthesis study of the white dwarf cooling sequence of the Galactic bulge that takes into account the populations of both single white dwarfs and binary systems containing at least one white dwarf. These calculations incorporate state-of-the-art cooling sequences for white dwarfs with hydrogen-rich and hydrogen-deficient atmospheres, for both white dwarfs with carbon–oxygen and helium cores, and also take into account detailed prescriptions of the evolutionary history of binary systems. Our Monte Carlo simulator also incorporates all the known observational biases. This allows us to model with a high degree of realism the white dwarf population of the Galactic bulge. We find that the observed excess of red stars can be partially attributed to white dwarf plus main sequence binaries, and to cataclysmic variables or dwarf novae. Our best fit is obtained with a higher binary fraction and an initial mass function slope steeper than standard values, as well as with the inclusion of differential reddening and blending. Our results also show that the possible contribution of double degenerate systems or young and thick-discbulge stars is negligible.

Key words: stars: luminosity function, mass function – white dwarfs – Galaxy: bulge – Galaxy: stellar content.

1 INTRODUCTION

White dwarfs are the most abundant fossil stars in the stellar graveyard. Actually, it turns out that more than 90 percent of all stars will end their evolution as white dwarfs. Moreover, their structural and evolutionary properties are reasonably well understood – see the review of Althaus et al. (2010) for an in depth discussion of this issue. Additionally, supported by the pressure of degenerate electrons, white dwarfs slowly cool down for periods of time, which are comparable to the age of the Galaxy. All this allows us to explore the evolution of various stellar systems at early times. As a matter of fact, the properties of the white dwarf population have been used as a valuable tool to study the nature and history of the different components of our Galaxy – including, for instance, the thin and thick discs (Winget et al. 1987; Garcia-Berro et al. 1988a,b; García-Berro et al. 1999; Torres et al. 2002; Rowell & Hambly 2011; Rowell 2013), and the Galactic halo (Mochkovitch et al. 1990; Isern et al. 1998; García-Berro et al. 2004; van Oirschot et al. 2014) – and the characteristics of several open and globular clusters – of which, to put some representative and recent examples, we mention the works of Calamida et al. (2008), García-Berro et al. (2010), Jeffery et al. (2011), Bono, Salaris & Gilmozzi (2013), Hansen et al. (2013), and Torres et al. (2015). Furthermore, the population of white dwarfs carries fundamental information about several crucial issues, like for instance (but not only) the amount of mass lost during the several evolutionary phases of their progenitors – see, for instance the recent review of García-Berro & Oswalt (2016). In addition, the population of white dwarfs can be used for other important purposes. We mention here three of them. First, the ensemble properties of the white dwarf population can be used to probe the behaviour of matter at large densities and low temperatures (Isern et al. 1991). White dwarfs can also be used to understand the evolution of planetary systems across the evolutionary life of their stars (Farihi 2016). Finally, the statistical properties of the population of Galactic white dwarfs have been successfully employed to corroborate or discard some non-standard physical theories (Isern, Hernanz & Garcia-Berro 1992; Garcia-Berro et al. 1995; Isern et al. 2008; García-Berro et al. 2011).

★ E-mail: Santiago.Torres@upc.edu (ST); calamida@stsci.edu (AC)
† Deceased 23rd September 2017.

Modern large-scale automated surveys, besides unveiling many new and interesting astronomical objects, are revolutionizing our understanding of the different Galactic populations. Specifically, the Sloan Digital Sky Survey (York et al. 2000), the Pan-STARRS collaboration (Kaiser et al. 2002), the RAVE Survey (Zwitter et al. 2008), or the SuperCosmos Sky Survey (Hambly et al. 1998), to cite a few examples, have provided us with an unprecedented wealth of astrometric and photometric data. Indeed, both the Sloan Digital Sky Survey and the SuperCosmos Sky Survey have increased the number of known white dwarfs belonging to the thin, thick and halo populations. Furthermore, a subset of these enhanced white dwarf samples has reliable determinations of their observable characteristics. All this has allowed us to undertake thorough studies of these three Galactic populations, aimed at uncovering their main properties.

However, because of the lack of observational data, this has not been possible yet for the Galactic bulge. Recently, a first sample of white dwarfs belonging to the Galactic bulge has been released (Calamida et al. 2014). Observations of the *Hubble Space Telescope* towards the low-reddening Sagittarius window in the Galactic bulge were deep enough to measure accurate magnitudes and proper motions for a sample of white dwarfs, allowing us to determine a relatively clean colour-magnitude diagram of the bulge (Calamida et al. 2014). The white dwarf cooling sequence contains ∼70 white dwarfs candidates. Moreover, Calamida et al. (2014) also identified ∼20 objects among extreme horizontal branch stars, dwarf novae and cataclysmic variables. However, a large spread in colour is observed with ∼30 per cent of the objects redder than expected for a typical carbon–oxygen white dwarf. This indicates that presumably there may be a substantial fraction of white dwarfs with helium cores, whose nature and origin remain to be elucidated. Here, we analyse, with the help of a Monte Carlo population synthesis code the observational data of this sample of stars, taking into account all the known observational biases and restrictions. We explore, among other issues, the nature of the observed population of red objects, the fraction of binaries and the population of double degenerates in the Galactic bulge.

Our paper is organized as follows. In Section 2, we describe with some detail the set of observations to which our theoretical simulations will be compared. Our numerical set up is briefly described in Section 3. The results of our Monte Carlo population synthesis calculations are described in full detail in Section 4. In particular, in Section 4.1, we discuss the properties of the population of single white dwarfs with carbon-oxygen cores. Section 4.2 is devoted to assess the possible existence of a sub-population of single helium white dwarfs, while in Section 4.3, we analyse the contribution of the sample of binary systems made of a carbon-oxygen white dwarf and a main-sequence star (WDMS). Other minor effects, differential reddening and blending are studied in Section 4.5. Finally, Section 5 is devoted to summarize our main results and to discuss their significance.

2 THE OBSERVED COLOUR–MAGNITUDE DIAGRAM

In Fig. 1, we present the colour–magnitude diagram of the sample of Calamida et al. (2014). The black points denote objects of the observed population, the open triangles are confirmed nova-like objects, and the black encircled points correspond to those objects that, according to Calamida et al. (2014) present photometric variability, and presumably are cataclysmic variables. The

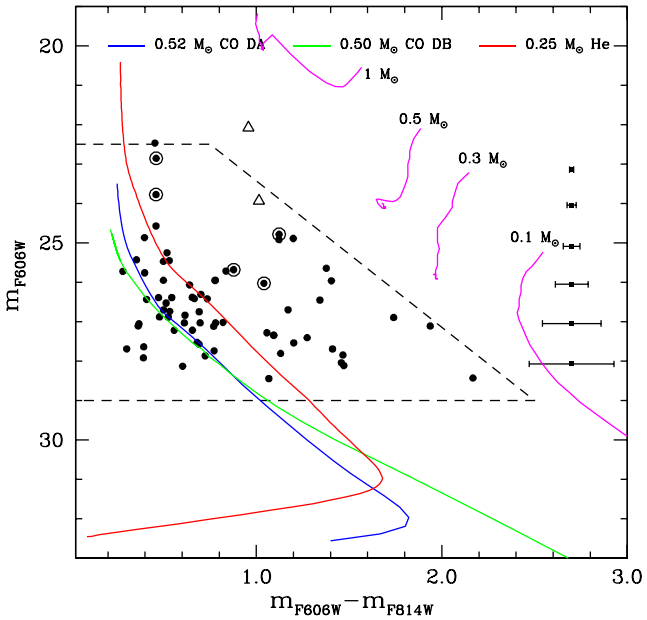

Figure 1. Color-magnitude diagram of the sample of Calamida et al. (2014) – black symbols. The encircled points are cataclysmic variable candidates, and the open triangles are confirmed nova-like objects. The dashed lines indicate the selection region of white dwarfs. Also plotted are different evolutionary sequences for white dwarf and main sequence stars as labeled. See text for details.

dashed lines delimit the selection region for white dwarfs in the colour–magnitude diagram. In particular, the bottom line indicates the limiting magnitude of the survey where the completeness of the sample drops below a 50 per cent. The upper line is the magnitude of the brightest white dwarfs according to the cooling tracks for carbon–oxygen white dwarfs at the distance and reddening of the bulge, while the oblique line represents the main-sequence blue edge. Also displayed in Fig. 1 are the theoretical cooling tracks for a 0.52 $M_{\odot}$ hydrogen-rich white dwarf with a carbon–oxygen core (Renedo et al. 2010) – blue line – a 0.50 $M_{\odot}$ carbon–oxygen white dwarf with a hydrogen-deficient atmosphere (Benvenuto & Althaus 1997) – green line – and a 0.25 $M_{\odot}$ white dwarf with helium core (Serenelli et al. 2001) – red line. These white dwarf masses correspond to the turn-off mass of the bulge for a typical age ∼11 Gyr. Clearly, although white dwarfs with helium cores are redder than regular carbon–oxygen white dwarfs, a region populated by even redder objects exits. Thus, objects in this region cannot be explained by the most up-to-date evolutionary stellar tracks, even when photometric errors are considered. A natural explanation for these stars is that they may be binary systems composed of a WDMS. To address this issue, and only for illustrative purposes, in Fig. 1, we have also plotted several evolutionary sequences for low-mass main-sequence stars (magenta lines) computed by Baraffe et al. (2015). These evolutionary sequences are plotted to show that the presence of a low-mass companion in a non-resolved binary system made of a main-sequence star and a white dwarf results in redder colours and brighter objects. Finally, note as well that within the region in the colour–magnitude diagram defined by the selection region of white dwarfs of the survey, the cooling tracks of white dwarfs with hydrogen rich and hydrogen deficient atmospheres do not differ by much.

3 BUILDING THE SYNTHETIC SAMPLE

The Monte Carlo population synthesis simulator employed in this work has been successfully used in several occasions. A thorough description of its main inputs can be found in García-Berro et al. (1999), Torres et al. (2002), and García-Berro et al. (2004). Consequently, here we will only describe its most relevant inputs, and we refer the interested reader to these works for detailed information of the rest of ingredients of the Monte Carlo code. For the calculations reported below, and except otherwise explicitly stated, we define a reference model with the following inputs. The mass of synthetic main-sequence stars is drawn randomly according to a Salpeter-like initial mass function with a standard slope, $\alpha = -2.35$, but below we explore other choices. The adopted age for our fiducial model of the bulge is $T_{\rm c} = 11.0$ Gyr with a constant burst of star formation lasting for 1 Gyr. An alternative model with a younger population is also studied in Section 4.4. The population of bulge stars has three sub-components of metallicities $Z = 0.03$, 0.02, and 0.008 (Haywood et al. 2016). We use a set of evolutionary sequences covering the full range of masses and metallicities of the progenitor stars of the white dwarf population (Renedo et al. 2010; Benvenuto & Althaus 1997; Serenelli et al. 2001). The set of cooling sequences for white dwarfs with pure hydrogen atmospheres was evolved self-consistently from the ZAMS, through the giant phase, the thermally pulsing AGB and mass-loss phases, and ultimately to the white dwarf cooling phase. All these sets of cooling sequences cover the full range of masses of interest. In the case of white dwarf main-sequence binaries, for the main-sequence companion, we employ the evolutionary tracks from Baraffe et al. (2015). These evolutionary sequences are valid for masses ranging from 0.07 to 0.5 $M_{\odot}$. A fraction, $f_{\rm BIN}$, of the total mass generated is evolved through binary systems following the prescriptions of Hurley, Tout & Pols (2002), with the improvements described in Camacho et al. (2014) and Cojocaru et al. (2017). Colours and magnitudes are transformed from the Johnson–Cousins system to the VEGAMAG zero-point magnitude system using the procedure of Sirianni et al. (2005). In our simulations, we adopt a distance modulus $(m - M)_0 = 14.45$ mag, a reddening $E(F606W - F814W) = 0.5766$ and an absorption $A_{F606W} = 1.4291$ mag (Calamida et al. 2014). The fraction of white dwarfs with hydrogen-rich atmospheres is 80 per cent, the canonical choice, while 20 per cent of stars are adopted to be white dwarfs with hydrogen deficient atmospheres. Finally, in order to strictly mimic the observational procedure, we implemented the corresponding magnitude and colour cuts of the survey, added the reported photometric errors and took into account the completeness of the sample.

4 RESULTS

4.1 The population of single white dwarfs

To start with, we discuss the population of single white dwarfs of the Galactic bulge. For this analysis, we selected stars in the sample of Calamida et al. (2014) that have photometry compatible with the expectations for single white dwarfs with carbon–oxygen cores. This was done by considering the region of the colour–magnitude diagram where a typical 0.52 $M_{\odot}$ white dwarf with hydrogen-rich atmosphere and with a carbon–oxygen core would be eventually found. This is the mass of the white dwarf for a progenitor with the main-sequence turn-off mass of $\approx$0.95 $M_{\odot}$. The corresponding cooling track for this mass is shown in Fig. 1 as a blue, solid line. We then added a conservative 1σ photometric error to this

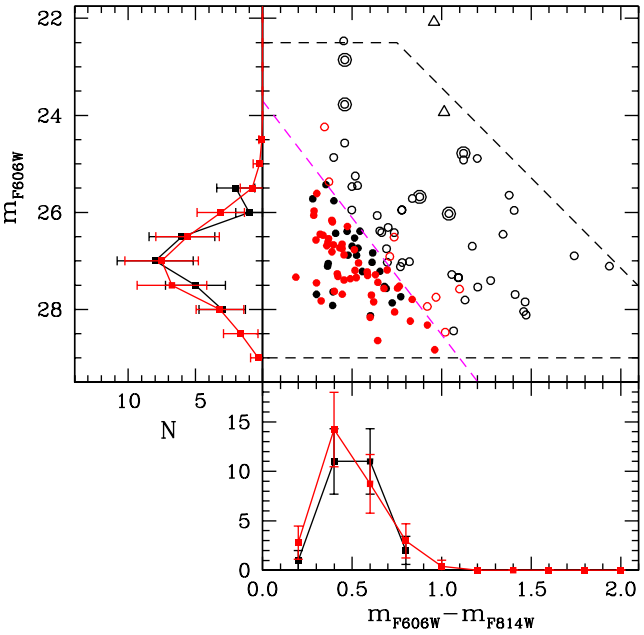

Figure 2. Colour–magnitude diagram (central panel) for the observed sample of Calamida et al. (2014) – black symbols – and for our simulated sample for the Galactic bulge single white dwarf population – red symbols. We assumed that objects bluer than the dividing line (magenta dashed line) are single white dwarfs. The corresponding luminosity function (left-hand panel) and colour distribution (bottom panel) for the observational (black lines) and simulated sample (red lines) are also shown. Excluded objects are marked with open symbols, while encircled points are cataclysmic variable candidates and open triangles are confirmed nova-like objects.

cooling sequence to obtain the region in the colour–magnitude diagram where these white dwarfs should be located. Objects with redder colours should be binary systems, or white dwarfs with helium cores, whatever their evolutionary origin could be. After this, we computed the magnitude distribution (that is, the white dwarf luminosity function) and the colour distribution. The results of this procedure are shown in Fig. 2. In particular, the central panel of this figure displays the colour–magnitude diagram of both the observed sample and of the simulated sample. Again, in this figure the dashed black lines indicate the selection region of white dwarfs of the survey. The dashed magenta line divides the regions in the colour–magnitude diagram, where single white dwarfs should be located (to the left-hand side of this line) and where with the highest probability binary systems or white dwarfs with helium cores are expected to lay (to the right-hand side of this line). Thus, filled red symbols are synthetic white dwarfs with carbon–oxygen cores and filled black symbols are the observed sample of white dwarfs with presumably carbon–oxygen cores. Open black symbols correspond to observed white dwarfs most likely having helium or belonging to binary systems, and hence are not used to obtain the white dwarf luminosity function and the colour distribution – see below. Finally, encircled symbols indicate those objects that were reported to be variable by Calamida et al. (2014). Now we turn our attention to the left-hand panel of this figure, which shows the observed (black line) and the synthetic (red line) white dwarf luminosity functions. As can be seen, despite the scarce number of observed stars, the agreement between the simulated and the observed sample is excellent. The same can be said regarding the colour distribution, see the bottom panel of Fig. 2. Thus, we conclude that our reference model, which

we remind was computed with a canonical ratio of 80 per cent of white dwarfs with hydrogen atmospheres and 20 per cent of white dwarfs with hydrogen-poor atmospheres, reproduces fairly well the population of single white dwarfs.

4.2 The population of white dwarfs with helium cores

Now we turn our attention to assess the existence of a population of single white dwarfs with helium cores. There is a general agreement that the vast majority of low-mass white dwarfs, namely those with $M_{\rm WD} \leq 0.47\,{\rm M}_{\odot}$, have evolved in binaries. Otherwise their low-mass main-sequence precursors would need more than the Hubble time to leave the main sequence. Moreover, Rebassa-Mansergas et al. (2011) analysed a large sample of short orbital period WD+MS binaries that evolved through a common envelope phase and provided robust observational evidence that the majority (∼85 per cent) of low-mass white dwarfs were formed as a consequence of mass transfer in binaries. However, the origin of the remaining ∼15 per cent of low-mass white dwarfs still lacks a consistent explanation. Several scenarios have been proposed. In particular, Type Ia supernova explosions in semidetached close binaries (Justham et al. 2009), severe mass-loss during the first giant branch phase (Kilic, Stanek & Pinsonneault 2007; Meng, Chen & Han 2008), ejection of the stellar envelope due to the spiral-in of close giant planets (Nelemans & Tauris 1998), or the merging of two extremely low-mass white dwarfs (Han et al. 2002), among other possible scenarios, have been proposed. Whatever the origin of these single white dwarfs with helium cores could be, they are redder than typical white dwarfs with carbon–oxygen cores. This becomes clear by examining Fig. 1, where we show using a solid red line the cooling track for a $0.25\,{\rm M}_{\odot}$ helium-core white dwarf.

To evaluate the impact of these white dwarfs in the white dwarf luminosity function and on the colour distribution of the white dwarf population of the Galactic bulge, we conducted a suite of simulations where we included a variable fraction, $f_{\rm He}$, of white dwarfs with helium cores. For an age of the bulge of 11 Gyr and adopting Solar metallicity, the turn-off mass is $\approx 1\,{\rm M}_{\odot}$ and the maximum mass of the progenitors that could have produced a helium-core white dwarf is $\approx 2\,{\rm M}_{\odot}$. Thus, we assumed that a fraction $f_{\rm He}$ ranging from 20 per cent to 50 per cent of main-sequence stars with masses in the interval between 1 and $2\,{\rm M}_{\odot}$ when they reach the giant branch produce a helium-core white dwarf with masses within the interval 0.25 and $0.45\,{\rm M}_{\odot}$. Even when the most extreme assumption is adopted, that is when a fraction $f_{\rm He} = 0.50$ is employed, our Monte Carlo simulations show that the probability of finding a single helium-white dwarf within the observed sample is far below 10^{-3}. Consequently, these stars do not contribute significantly to the number counts, and thus their impact on the magnitude and colour distributions is totally negligible. In principle, we need to consider that several non-linear causes are present in this final low probability, such as a non-constant initial mass function or a spread in born-ages due to the 1 Gyr burst. However, we point out that the main reason for this result is that helium-core white dwarfs cool down much faster than regular white dwarfs with carbon–oxygen cores. In particular, the time needed for a typical $0.25\,{\rm M}_{\odot}$ helium-core white dwarf to cross the region within the selection limits of white dwarfs of the survey – which correspond to effective temperatures between ≈27 500 and ≈4 500 K – is less than ∼4.4 Gyr, while for a typical $0.6\,{\rm M}_{\odot}$ white dwarf with a carbon–oxygen core is ∼9.1 Gyr.

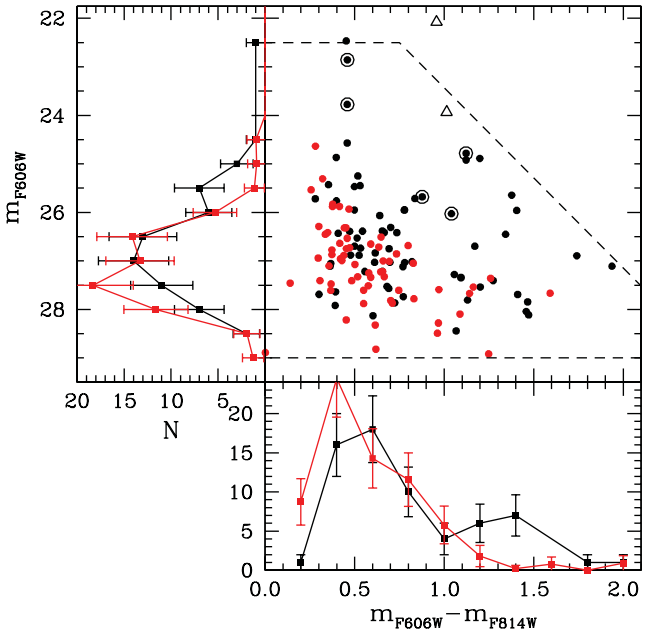

Figure 3. Same as Fig. 2 but for the population of single and binary white dwarfs of the Galactic bulge. Our simulated sample (red symbols and red lines) corresponds to Model 1.

4.3 The binary white dwarf population

The analysis done in the previous section also demonstrates that a significant fraction of objects in the observed sample – namely those with colours redder than usual – are probably binary systems. This percentage is ∼63 per cent, a high value. To verify if this hypothesis is correct, we assumed that a fraction $f_{\rm BIN}$ of the total mass generated in the theoretical simulations goes to form binaries, and we kept all other inputs fixed, including the initial mass function. Starting with a canonical value of $f_{\rm BIN} = 0.50$ – we refer this model as Model 0 – we increased $f_{\rm BIN}$ so that the final percentage of binaries is maximize but keeping a good fit for the luminosity function and colour distribution of the single white dwarf sample. Specifically, we assumed that this fraction is $f_{\rm BIN} = 0.80$. Additionally, we explored other choices of the initial mass function, as well as other options for the age spread. We assumed that the initial distribution of mass ratios of the primary and secondary stars, $n(q)$ where $q = M_2/M_2$, and M_1 and M_2 are the masses of the primary and secondary members of the pair, respectively, is flat. We also adopted a value for the envelope efficiency $\alpha_{\rm CE} = 0.3$, with no internal energy contribution $\alpha_{\rm int} = 0.0$, in accordance with the results of Camacho et al. (2014), and with all these inputs we generated a sample of synthetic binaries. From now on we will refer to this model as Model 1.

In Fig. 3, we present the results of this model, and we compare them with the full sample of Calamida et al. (2015). As we did previously, we employ black symbols to represent the observational data. We emphasize that now the white dwarf luminosity function and the colour distribution – see below – have been computed taking into account all the white dwarfs observed by Calamida et al. (2014), not only those white dwarfs that are single and with carbon–oxygen cores, as we did previously (in Section 4.1). Comparing Figs 2 and 3, it is quite apparent that the observed luminosity function (left-hand panel, black line) and the colour distribution (bottom panel, black line) of the full sample of white dwarfs have secondary peaks that were not present in the luminosity function and colour distribution of Fig. 2. These secondary peaks are located at magnitude

Table 1. Models of the binary population used in this work. Lasts columns show the final percentages obtained for the populations of single white dwarfs, double degenerates and WDMS pairs, respectively, and the reduced χ^2_ν value for the luminosity function and the color distribution, respectively.

Model	$f_{\rm BIN}$	$\alpha_{\rm CE}$	$\alpha_{\rm int}$	$n(q)$	$\alpha_{\rm IMF}$	per cent WD	per cent DD	per cent WD+MS	$\chi^2_{\nu,\rm LF}$	$\chi^2_{\nu,\rm CD}$
0	0.5	0.3	0.0	1	−2.35	97.5	0.0	2.5	1.13	2.13
1	0.8	0.3	0.0	1	−2.35	90.3	1.4	8.3	1.05	2.14
2	0.8	0.3	0.0	1	−2.55	90.0	0.5	9.5	1.09	1.91
3	0.8	0.3	0.0	1	−2.15	89.0	2.8	8.2	1.15	2.13
4	0.8	1.0	0.1	1	−2.35	90.1	1.4	8.4	1.10	2.06
5	0.8	0.3	0.0	q	−2.35	94.1	0.0	5.9	1.11	1.88
6	0.8	0.3	0.0	q^{-1}	−2.35	82.5	2.0	15.5	0.87	1.81
7	0.8	1.0	0.1	Duquennoy & Mayor (1991)	Kroupa (2001)	87.8	2.7	9.5	0.83	1.61
8	0.8	1.0	0.1	q^{-1}	−2.55	77.9	1.0	21.1	1.09	1.17

$m_{F606W} \approx 25.5$ for the luminosity function and at colour $(m_{F606W} - m_{F814W}) \approx 1.4$ for the colour distribution, respectively. Naturally, this is due to the red objects that we did not consider in our previous analysis. Finally, the synthetic stars resulting from Model 1 are shown in the central panel of Fig. 3 using red symbols. Examining this figure is evident that Model 1, that we remind considers the population of WDMS, is not able to reproduce the main features of the observed colour–magnitude diagram. Consequently, the theoretical white dwarf luminosity function (left-hand panel, red line) and the colour distribution (bottom panel, red line) do not match the observed distributions. Specifically, Fig. 3 clearly demonstrates that the synthetic population of Model 1 does not reproduce the secondary peaks of the observed distributions. Indeed, although this model produces some objects that are redder than usual, the fraction of these objects is 8.3 per cent, far below the percentage of these objects in the observed sample.

Thus, an alternative model must be sought. Consequently, we explore a suite of models aimed to obtain a larger fraction of WDMS pairs. The different models studied here are listed in Table 1. The first column displays the model, being Model 1 our reference model. In the next columns, the values of $\alpha_{\rm CE}$, $\alpha_{\rm int}$, $n(q)$, $\alpha_{\rm IMF}$, and the percentages of the single stars, double degenerate binaries and WDMS pairs of the synthetic sample are listed. For a quantitative comparison of the models, the reduced χ^2_ν test value of the luminosity function and the colour distribution was calculated. Defined as $\chi^2_\nu = \chi^2/\nu$ where ν is the degree of freedom of the respective function, the corresponding results are shown in the last two columns of Table 1. Models 2 to 6 are slight variants of Model 1. For these models, only one parameter is modified. In particular, Models 2 and 3 are intended to explore the slope of the initial mass function. In Model 4, we explore the role of the free parameters of the common envelope phase. Finally, Models 5 and 6 are thought to explore the effects of $n(q)$, the distribution of mass ratios within the binary system. Model 7 is the model that best fits the mass function of the Galactic bulge (Calamida et al. 2015). In particular, we use for this model the log-normal distribution of mass ratios of binary stars of Duquennoy & Mayor (1991) and the initial mass function of Kroupa (2001). In short, the results shown in this table show that larger percentages of WDMS pairs are produced when a decreasing binary mass ratio distribution is adopted (Model 6), and when a larger common envelope efficiency with internal energy are adopted. Also, we find that a steeper slope for the initial mass function fits better the distribution of masses of Calamida et al. (2015). Finally, Model 8 is tailored to maximize the percentage of synthetic binary systems. For this particular model, the percentage of binary systems is the largest, 21 per cent. Besides we can check that the reduced χ^2 value is the closest to 1 of all models, thus concluding that Model 8 fits better the white dwarf luminosity function and the colour distribution. The corresponding luminosity function, magnitude–colour diagram and colour distribution are shown in Fig. 4. However, our simulations also reveal that there is a region of the colour–magnitude diagram where our simulations do not yield any binary system, at odds with what is observationally found.

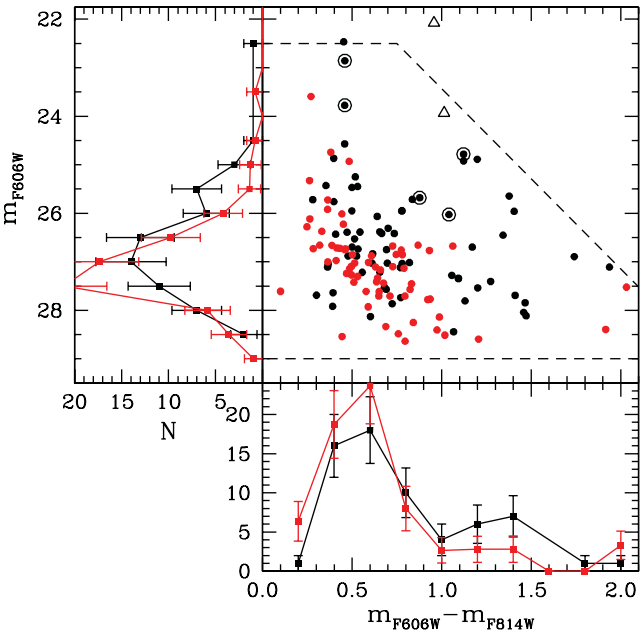

Figure 4. Same as Fig. 2 but for the population of single and binary white dwarfs of the Galactic bulge. The simulated sample (red symbols and red lines) is that of Model 8.

To study which systems may eventually be found in the region of the colour–magnitude diagram that our simulations are not able to populate, in Fig. 5 we show density maps of the region of the magnitude–colour diagram populated by the population of single white dwarfs (top panel), the WDMS population (central panel) and the population of double degenerate systems (bottom panel), obtained using Model 8. It is interesting to note that the bulk of the different subpopulations lays outside of the observed region. For instance, the vast majority of single white dwarfs have cooled down to magnitude $m_{F606W} \approx 31.5$, far below the completeness limit of the sample. On the other hand, WDMS systems have magnitudes within the selection region of white dwarfs of the survey; however, their colours are considerably redder than the observational colour cut.

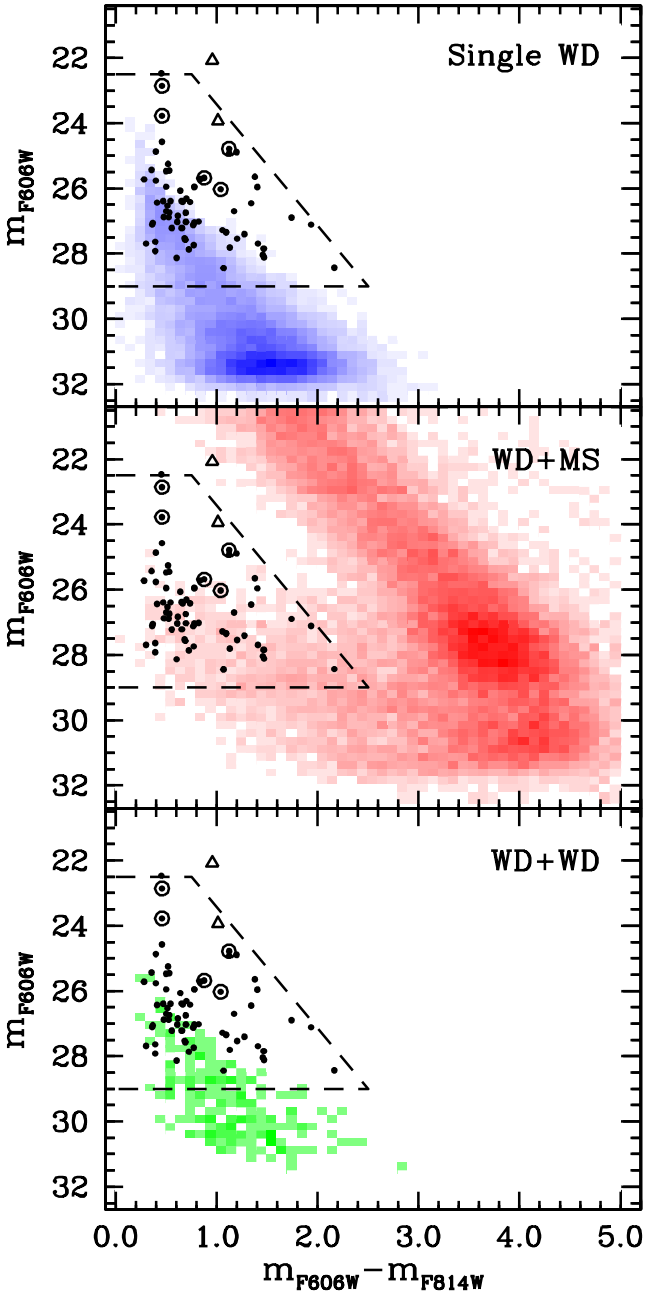

Figure 5. Density map of the Galactic bulge populations of single white dwarfs (top panel), white dwarf plus main-sequence binaries (central panel) and double-degenerate systems (bottom panel). The results plotted here are those of our Model 8, which maximizes the fraction of binaries.

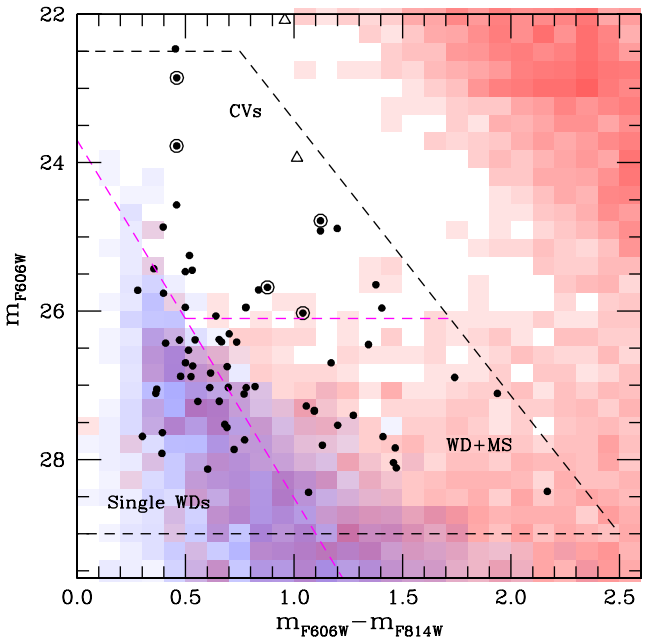

Figure 6. Same as Fig. 2, but combining the population of single and binary white dwarfs of the Galactic bulge. The magenta lines indicate the regions where the populations of single white dwarfs and WDMS systems, respectively, are dominant, as labelled. The results presented in this figure are those obtained using Model 8.

Consequently, only objects of the respective tails of the distributions are culled. Finally, the contribution of double degenerate systems is quite marginal and can be safely disregarded given that they represent no more than a 2 per cent of the systems in the observable window.

In Fig. 6, a density map of the observable region of the colour–magnitude diagram for the entire synthetic population, weighted by their relative contribution to the final sample is shown. As can be seen, within the observable window of the colour–magnitude diagram the different populations overlap. Clearly, the observed sample is dominated by the single white dwarf sub-sample (blue colour) and by the WDMS population (red colour), while the contribution of double white dwarf systems is negligible. Taking into account which is the largest percentage of the different populations, the observable region can be divided in smaller regions. The magenta dashed lines in Fig. 6 show the limits of these regions. Basically, the region explored by Calamida et al. (2014) can be divided in three regions. Objects with colours $m_{F606W} - m_{F814W} \lesssim 1.0$ and magnitudes ranging from $m_{F606W} \simeq 29$ to 24 are predominantly single white dwarfs. Observed objects with magnitudes between 29 and ∼26 and colours redder than those of the magenta dashed line are most likely WDMS systems. The only region that our simulations are not able to cover is objects brighter than magnitude 26 and colours redder than that of the magenta dashed line. This means these objects should be cataclysmic variables or dwarf novae, since we are left with no other option. Moreover, it is worth mentioning that Calamida et al. (2014) found convincing evidence for variability of a sizable fraction of objects in this region. Although we cannot use this approach to assign a membership to each individual object in the sample of Calamida et al. (2014), we can roughly estimate the nature of the observed sample. According to our simulations, ∼40 per cent of the observable sample are probably single white dwarfs, ∼38 per cent are WDMS systems, and nearly ∼22 per cent are cataclysmic variables or dwarf novae.

Finally, we discuss the properties of the population of WDMS binaries that contribute to the observed sample. In the top panel of Fig. 7, we show the mass of the main-sequence star as a function of the mass of the white dwarf companion. As can be seen two formation channels coexist. The main channel, which accounts for ∼67 per cent of the binary systems, produces a ∼0.54 $M_\odot$ carbon–oxygen white dwarf and a low-mass main-sequence star with a mass ranging from 0.1 to 0.3 $M_\odot$. The second channel, which accounts for the rest of the binary systems, results in a white dwarf with a helium core and mass between 0.3 and 0.44 $M_\odot$, and a low-mass main-sequence companion with mass in the interval 0.1 to

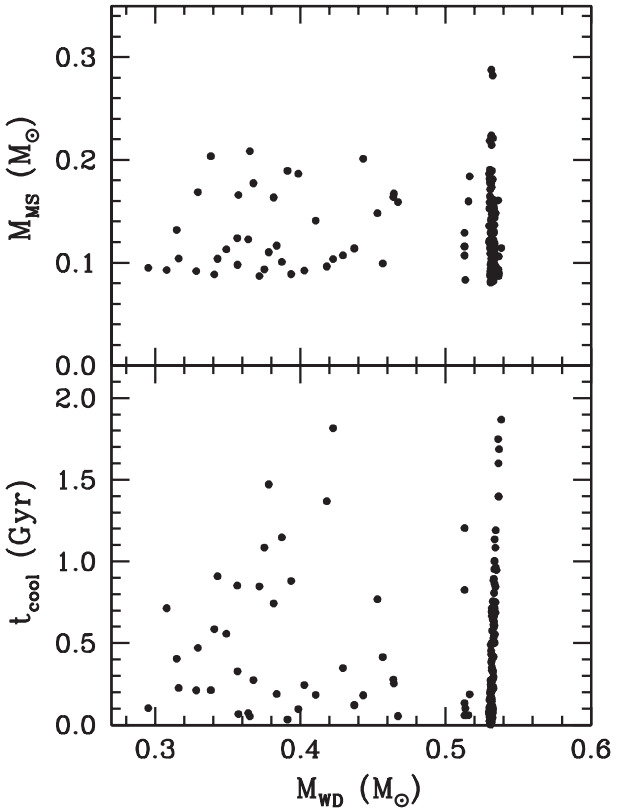

Figure 7. Main-sequence mass as a function of the white dwarf mass (top panel) and cooling age of the white dwarf as a function of its mass (bottom panel) for those WDMS systems that lay in the observational window of Calamida et al. (2015). The data presented in this figure are those resulting from Model 8.

$0.2\,M_\odot$. Naturally, this also results in different cooling times for both formation channels. This is illustrated in the bottom panel of the same figure, where the white dwarf cooling times of the member of the pair are shown as a function of its mass. It is worth emphasizing that for both formation channels the white dwarf cooling ages are shorter than 2 Gyr. This indicates that the WDMS systems must be made of relatively hot white dwarfs to enter into the observational sample, otherwise the colour of the system would be dominated by the main-sequence companion, and consequently it would be redder.

4.4 A young bulge population?

The origin of the bulge still remains controversial. While there exists a general consensus that the vast majority of the bulge population is uniformly old, there is some evidence for a significant younger population – see Haywood et al. (2016), and references therein. The observed bar-like shape of the Galaxy seems to be clearly connected to the thick disc structure and, consequently, the observed dispersion in metallicities of the bulge stars can be associated with the different stellar populations of the Galaxy (Di Matteo 2016). To check whether a younger bulge population has noticeable effects on the results presented until now, we ran an additional simulation to take into account a younger population. In particular, we slightly modified Model 8 to include a star formation rate history, which incorporates a young population. We adopt a simplified model that reasonably resembles that of Haywood et al. (2016) – see their Fig. 1 for details. That is, to the burst of star formation of duration 1 Gyr

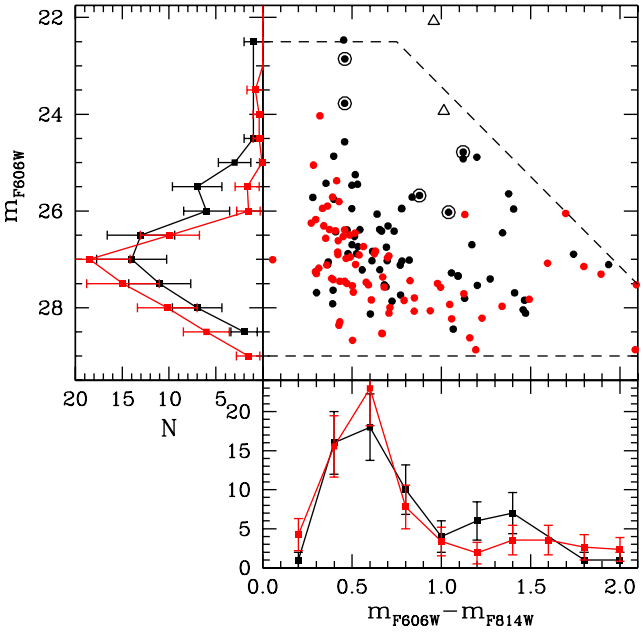

Figure 8. Same as Fig. 4 but for a star formation history that includes a young bulge population.

that occurred 11.0 Gyr ago and produced stars with low metalicity we added a constant formation period, lasting until the present, of metal-rich stars with a formation rate 20 per cent of that of that of the burst.

The results of employing this star formation history are displayed in Fig. 8. As in Fig. 4, we show our simulated sample (black symbols and black solid lines) compared to the observational data set (red dots and solid red lines). First, it is important to mention that including a younger population of stars substantially increases the number of WDMS binaries in the final sample. Specifically, we obtain that when this star formation rate is employed the fraction of WDMS binaries climbs to 31 per cent of the total synthetic population. However, even though the number of objects redder than usual increases – so we obtain a better fit to the colour distribution (see the bottom panel of Fig. 8) – the white dwarf luminosity function (see the left panel of Fig. 8) is clearly shifted towards fainter magnitudes – the respective reduced χ^2 values are: $\chi^2_{\nu,\mathrm{CD}} = 1.34$ and $\chi^2_{\nu,\mathrm{LF}} = 2.41$. This excess of faint white dwarfs prevents us to adopt models of the Galactic bulge with a significant fraction of young objects. Actually, we conducted a set of additional simulations to explore the maximum possible contribution of this putative young population and found that the sample of Calamida et al. (2014) restricts its contribution to a modest 5 per cent of the standard old population. This is the same to say that the mass of the young population should be less than 33 per cent of the total mass of the Galactic bulge. In summary, our results indicate that this population is not only unable to explain the presence of anomalous red objects in the sample of bulge white dwarfs, but also is at odds with the observed white dwarf luminosity function, unless its contribution is almost negligible.

4.5 Differential reddening and blending

In previous sections, we have established that the population of WDMS is the main contributor to the observed population of red objects of the Galactic bulge sample. However, even when a model that maximizes the presence of binaries is employed, some

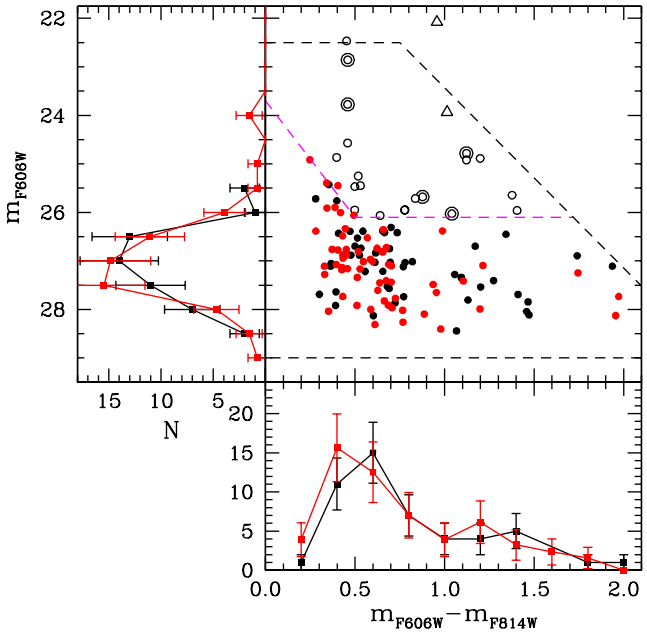

Figure 9. Same as Fig. 2 but for the population of single and binary white dwarfs of the Galactic bulge. Our simulated sample (red symbols and red lines) is that of Model 8, but adding differential reddening and 10 per cent of blended objects. The exclusion region of variable objects is shown using a dashed magenta line.

discrepancies between the simulated and observed sample persist. In the following we analyse two possibilities that could help in alleviating these discrepancies, namely differential reddening and blending. Nevertheless, we advance that we foresee that the inclusion of these two effects will have a minor impact on the results.

First, we include in Model 8 differential reddening. It is well known that dense molecular clouds towards the Galactic centre exist. These molecular clouds produce a spatially variable extinction. Disentangling the contribution of differential reddening for each individual object in the observed sample is a quite unfordable task, which is beyond the scope of the present study. However, we can estimate the effect of differential reddening using our Monte Carlo simulated samples. To do this, we follow closely the work of Calamida et al. (2014). Specifically, to simulate differential reddening in the Sagittarius window, we assume the presence of random clumps of full width at half-maximum of ≈5 arcsec (in total 500 clumps fit in the ACS images) with a reddening increase of $E(F606W-F814W)=0.228$ ($A_{F606W}=1.4291$ mag) on the top of a uniform reddening of $E(F606W-F814W)=0.5766$.

In addition to the possible effects of differential reddening, we also consider that a small fraction of objects belong to unresolved pairs. This is a reasonable assumption, since the observed fields are crowded. In particular, white dwarf artificial tests indicate that the percentage of blended stars could be as high as ∼10 per cent (Calamida et al. 2014), which is the value we adopt here.

The results for our best model (Model 8) when differential reddening and blending effects are taken into account are shown in Fig. 9. To perform the analysis of the simulated sample, we exclude from the white dwarf luminosity function and the colour distribution those objects that presumably are variable. The boundaries of the corresponding region in the colour–magnitude diagram are represented in Fig. 9 employing magenta dashed lines. Clearly, the agreement between the observed (black lines) and simulated results (red lines) is now noticeably good. That is quantitative corroborate by reduced χ^2 values close to 1 for the luminosity function and the colour distribution, $\chi^2_{\nu,\rm LF}=1.05$ and $\chi^2_{\nu,\rm CD}=1.16$, respectively. It is worth saying that, even though differential reddening and unresolved pairs are not by their own able to explain the redder region of the observed colour–magnitude diagram of the sample of Calamida et al. (2014), their inclusion in our models clearly improves the fit.

5 CONCLUSIONS

Using an state-of-the-art Monte Carlo simulator, which includes the population of single and binary white dwarfs and the most up-to-date evolutionary sequences, we have studied the observational sample of the Galactic bulge of Calamida et al. (2014). Our reference model with a canonical ratio of white dwarfs with hydrogen-rich to hydrogen-deficient atmospheres reproduces fairly well the single white dwarf population of the galactic bulge, but is not able to reproduce other features of the colour–magnitude diagram, and, in particular, could not reproduce the observed excess of red objects. Consequently, we sought for other alternatives. We first analysed the possibility of these objects being members of a population of single helium-core white dwarfs. However, we found that the observed excess of red stars in the colour–magnitude diagram cannot be attributed to this population. We then studied the possibility of these objects being members of binaries. We found that our Monte Carlo simulations including the binary white dwarf population reproduce better the gross features of the colour–magnitude diagram, there are still some objects that cannot be reproduced by the population of white dwarf plus main-sequence binaries, because their colours are bluer and they are fainter than their observed counterparts, nor by a population of double degenerate binaries, because its contribution is smaller than 2 per cent, too small to account for the observed number of objects. Thus, the only explanation we are left with is that these bright and red objects are cataclysmic variables or dwarf novae. This explanation agrees with the hypothesis put forward by Calamida et al. (2014), who found that some of these objects present variability. However, follow-up observations will be needed to fully confirm this scenario. Once, the putative population of cataclysmic variables is eliminated from the colour–magnitude diagram we obtain a nice fit to both the white dwarf luminosity function and to the colour distribution, when a fraction $\lesssim 10$ per cent of blended objects is included in the models. The best fit is obtained when $\alpha_{\rm CE}=1$, $\alpha_{\rm int}=0.1$, $n(q)=q^{-1}$, $\alpha_{\rm IMF}=-2.55$, and $f_{\rm BIN}\simeq 0.80$ are adopted, and differential reddening and blending are included. Although we cannot rule out the contribution of young and thick-disc metallicity bulge stars, we placed an upper limit to their contribution to the mass budget of the Galactic bulge, and we found that it must be smaller than 33 per cent of the total bulge mass.

ACKNOWLEDGEMENTS

This work was partially supported by MINECO grant AYA2011–23102.

REFERENCES

Althaus L. G., Córsico A. H., Isern J., García-Berro E., 2010, A&A Rev., 18, 471
Baraffe I., Homeier D., Allard F., Chabrier G., 2015, A&A, 577, A42
Benvenuto O. G., Althaus L. G., 1997, MNRAS, 288, 1004
Bono G., Salaris M., Gilmozzi R., 2013, A&A, 549, A102
Calamida A. et al., 2008, ApJ, 673, L29
Calamida A. et al., 2014, ApJ, 790, 164

Calamida A. et al., 2015, ApJ, 810, 8
Camacho J., Torres S., García-Berro E., Zorotovic M., Schreiber M. R., Rebassa-Mansergas A., Nebot Gómez-Morán A., Gänsicke B. T., 2014, A&A, 566, A86
Cojocaru R., Rebassa-Mansergas A., Torres S., Garcia-Berro E., 2017, MNRAS, 470, 1442
Di Matteo P., 2016, PASA, 33, e027
Duquennoy A., Mayor M., 1991, A&A, 248, 485
Farihi J., 2016, New A Rev., 71, 9
García-Berro E., Oswalt T. D., 2016, New A Rev., 72, 1
Garcia-Berro E., Hernanz M., Mochkovitch R., Isern J., 1988a, A&A, 193, 141
Garcia-Berro E., Hernanz M., Isern J., Mochkovitch R., 1988b, Nature, 333, 642
Garcia-Berro E., Hernanz M., Isern J., Mochkovitch R., 1995, MNRAS, 277, 801
García-Berro E., Torres S., Isern J., Burkert A., 1999, MNRAS, 302, 173
García-Berro E., Torres S., Isern J., Burkert A., 2004, A&A, 418, 53
García-Berro E. et al., 2010, Nature, 465, 194
García-Berro E., Lorén-Aguilar P., Torres S., Althaus L. G., Isern J., 2011, J. Cosmol. Astropart. Phys., 5, 021
Hambly N. C., Miller L., MacGillivray H. T., Herd J. T., Cormack W. A., 1998, MNRAS, 298, 897
Han Z., Podsiadlowski P., Maxted P. F. L., Marsh T. R., Ivanova N., 2002, MNRAS, 336, 449
Hansen B. M. S. et al., 2013, Nature, 500, 51
Haywood M., Di Matteo P., Snaith O., Calamida A., 2016, A&A, 593, A82
Hurley J. R., Tout C. A., Pols O. R., 2002, MNRAS, 329, 897
Isern J., Hernanz M., Mochkovitch R., Garcia-Berro E., 1991, A&A, 241, L29
Isern J., Hernanz M., Garcia-Berro E., 1992, ApJ, 392, L23
Isern J., García-Berro E., Hernanz M., Mochkovitch R., Torres S., 1998, ApJ, 503, 239
Isern J., García-Berro E., Torres S., Catalán S., 2008, ApJ, 682, L109
Jeffery E. J., von Hippel T., DeGennaro S., van Dyk D. A., Stein N., Jefferys W. H., 2011, ApJ, 730, 35
Justham S., Wolf C., Podsiadlowski P., Han Z., 2009, A&A, 493, 1081
Kaiser N. et al., 2002, in Tyson J. A., Wolff S., eds, Proc. SPIE Conf. Ser. Vol. 4836, Survey and Other Telescope Technologies and Discoveries. SPIE, Bellingham, p. 154
Kilic M., Stanek K. Z., Pinsonneault M. H., 2007, ApJ, 671, 761
Kroupa P., 2001, MNRAS, 322, 231
Meng X., Chen X., Han Z., 2008, A&A, 487, 625
Mochkovitch R., Garcia-Berro E., Hernanz M., Isern J., Panis J. F., 1990, A&A, 233, 456
Nelemans G., Tauris T. M., 1998, A&A, 335, L85
Rebassa-Mansergas A., Nebot Gómez-Morán A., Schreiber M. R., Girven J., Gänsicke B. T., 2011, MNRAS, 413, 1121
Renedo I., Althaus L. G., Miller Bertolami M. M., Romero A. D., Córsico A. H., Rohrmann R. D., García-Berro E., 2010, ApJ, 717, 183
Rowell N., 2013, MNRAS, 434, 1549
Rowell N., Hambly N. C., 2011, MNRAS, 417, 93
Serenelli A. M., Althaus L. G., Rohrmann R. D., Benvenuto O. G., 2001, MNRAS, 325, 607
Sirianni M. et al., 2005, PASP, 117, 1049
Torres S., García-Berro E., Burkert A., Isern J., 2002, MNRAS, 336, 971
Torres S., García-Berro E., Althaus L. G., Camisassa M. E., 2015, A&A, 581, A90
van Oirschot P., Nelemans G., Toonen S., Pols O., Brown A. G. A., Helmi A., Portegies Zwart S., 2014, A&A, 569, A42
Winget D. E., Hansen C. J., Liebert J., van Horn H. M., Fontaine G., Nather R. E., Kepler S. O., Lamb D. Q., 1987, ApJ, 315, L77
York D. G. et al., 2000, AJ, 120, 1579
Zwitter T. et al., 2008, AJ, 136, 421

This paper has been typeset from a TEX/LATEX file prepared by the author.